Change detection in a series of Sentinel-1 SAR data

Allan A. Nielsen[1], Knut Conradsen[1], Henning Skriver[2] and Morton J. Canty[3]

[1]DTU Compute – Applied Mathematics and Computer Science
[2]DTU Space – National Space Institute
Technical University of Denmark
DK-2800 Kgs. Lyngby, Denmark
[3]Research Center Juelich
D-52425 Juelich, Germany

***Abstract*—Based on an omnibus likelihood ratio test statistic for the equality of several variance-covariance matrices following the complex Wishart distribution with an associated p-value and a factorization of this test statistic, change analysis in a time series of seven multilook, dual polarization Sentinel-1 SAR data in the covariance matrix representation (with diagonal elements only) is carried out. The omnibus test statistic and its factorization detect if and when change occurs.**

http://www.imm.dtu.dk/pubdb/p.php?6982.

I. Introduction

Based on work reported in [1], this contribution detects change in a series of (seven) Sentinel-1[1] dual polarization (here covariance matrix representation, [2], VV/VH, diagonal only) C-band synthetic aperture radar (SAR) data sets over Frankfurt Airport. In [3], [4] we worked with bitemporal change detection in polarimetric SAR data by means of a test statistic in the complex Wishart distribution. In [5] the bitemporal change detection problem in polarimetric SAR data is dealt with by means of the Hotelling-Lawley trace statistic. For more references to change detection in polarimetric SAR data and for further mathematical detail, see [1]. The account given here closely follows [6].

II. Omnibus change detection method

The Sentinel-1 data are dual polarization. In the covariance matrix representation each pixel at each time point is a matrix

$$\langle \boldsymbol{C} \rangle_{dual} = \begin{bmatrix} \langle S_{vv}S_{vv}^* \rangle & \langle S_{vv}S_{vh}^* \rangle \\ \langle S_{vh}S_{vv}^* \rangle & \langle S_{vh}S_{vh}^* \rangle \end{bmatrix}.$$

In our case we have the diagonal elements only. The matrix with the off-diagonal elements set to zero does not follow a complex Wishart distribution but the two (1 by 1) "blocks" on the diagonal do [3], [7], [8], [1]. The "block" $\langle S_{vv}S_{vv}^* \rangle$ is 1 by 1, $p_1 = 1$, and the "block" $\langle S_{vh}S_{vh}^* \rangle$ is 1 by 1, $p_2 = 1$.

For the logarithm of the so-called omnibus test statistic Q for no change between all k time points introduced in [1] (which deals with complex data, for the real case, see [9]), we get

$$\ln Q = n\{pk \ln k + \sum_{i=1}^{k} \ln |\boldsymbol{X}_i| - k \ln |\sum_{i=1}^{k} \boldsymbol{X}_i|\}. \quad (1)$$

Here $p = p_1 + p_2 = 2$ and $\boldsymbol{X}_i = n\langle \boldsymbol{C} \rangle_{dual}$ where n is the equivalent number of looks. $|\cdot|$ denotes the determinant.

For the test statistic R_j, that given no change between the first $j-1$ time points, we have no change between time points $j-1$ and j, we get

$$\ln R_j = n\{p(j \ln j - (j-1)\ln(j-1)) + (j-1)\ln|\sum_{i=1}^{j-1} \boldsymbol{X}_i| + \ln|\boldsymbol{X}_j| - j \ln|\sum_{i=1}^{j} \boldsymbol{X}_i|\}. \quad (2)$$

The R_j constitute a factorization of Q, i.e., $Q = \prod_{j=2}^{k} R_j$ or

$$\ln Q = \sum_{j=2}^{k} \ln R_j. \quad (3)$$

The distributions of the $-2\ln R_j$ and $-2\ln Q$ test statistics under the assumption of no change are approximately χ^2 with $f = p_1^2 + p_2^2 = 2$ and $(k-1)f$ degrees of freedom, respectively. Better approximations for dual and full polarization data (for the full matrix case) are given in [1].

With this method we build a structure of change for each pixel: first we look at change over all time points, then at change over all time points omitting the first time point, then at change over all time points omitting the first two time points, etc. The change structure is illustrated in Table I. Note that the pairwise tests for comparison between t_i and t_{i+1}, $R_2^{(i)}$, appear on the diagonal.

If change is detected comparing for example t_2 and t_3 in the "$t_1 = \cdots = t_7$" column in Table I, the remaining tests in that column are invalid and we continue in the column starting with detection of change from t_3. This will leave the "$t_2 = \cdots = t_7$" column irrelevant. Continuing like this we can build up the change pattern for all pixels over all time points, see also [1], [10].

III. Sentinel-1 data, Frankfurt Airport

The data used in this study are from the Sentinel-1 dual polarization (here VV/VH, diagonal only) C-band SAR instrument. Seven scenes (all ascending node and all with relative orbit number 15) covering the international airport in Frankfurt, Germany, are obtained from Google Earth Engine[2]

http://people.compute.dtu.dk/alan, alan@dtu.dk.

[1]https://sentinel.esa.int/web/sentinel/missions/sentinel-1.

[2]https://earthengine.google.com and https://developers.google.com/earth-engine.

978-1-5386-3327-4/17/$31.00

TABLE I. ILLUSTRATION OF THE CHANGE STRUCTURE FOR DATA FROM SEVEN TIME POINTS.

	$t_1 = \cdots = t_7$	$t_2 = \cdots = t_7$	$t_3 = \cdots = t_7$	$t_4 = \cdots = t_7$	$t_5 = t_6 = t_7$	$t_6 = t_7$
Omnibus	$Q^{(1)}$	$Q^{(2)}$	$Q^{(3)}$	$Q^{(4)}$	$Q^{(5)}$	$Q^{(6)}$
$t_1 = t_2$	$R_2^{(1)}$					
$t_2 = t_3$	$R_3^{(1)}$	$R_2^{(2)}$				
$t_3 = t_4$	$R_4^{(1)}$	$R_3^{(2)}$	$R_2^{(3)}$			
$t_4 = t_5$	$R_5^{(1)}$	$R_4^{(2)}$	$R_3^{(3)}$	$R_2^{(4)}$		
$t_5 = t_6$	$R_6^{(1)}$	$R_5^{(2)}$	$R_4^{(3)}$	$R_3^{(4)}$	$R_2^{(5)}$	
$t_6 = t_7$	$R_7^{(1)}$	$R_6^{(2)}$	$R_5^{(3)}$	$R_4^{(4)}$	$R_3^{(5)}$	$R_2^{(6)}$

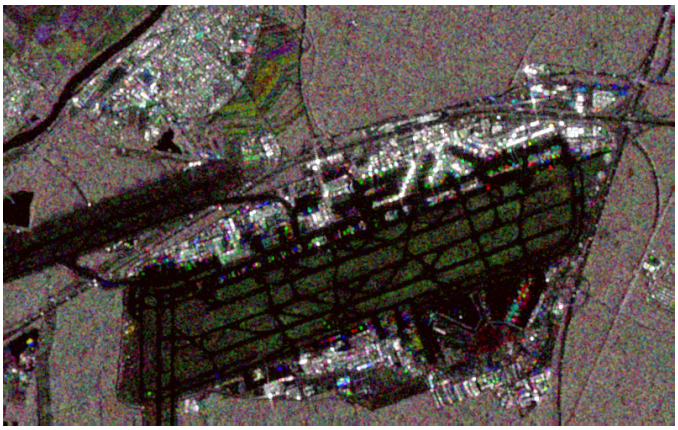

Fig. 1. RGB image of Sentinel-1 C-band multi-temporal VH data, 10 Feb 2016 as R, 15 Jul 2016 as G, and 12 Nov 2016 as B,10 m pixels, 5 km north-south and 8 km east-west, all three bands are stretched linearly between -24 dB and 0 dB.

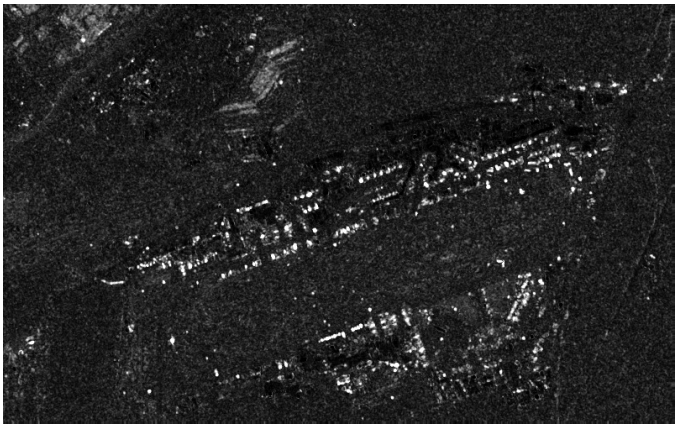

Fig. 2. $-2\ln Q$ omnibus change detector for Sentinel-1 C-band VV/VH dual polarization data, diagonal only, over seven time points from 10 Feb 2016 through 12 Nov 2016, stretched linearly between 0 and 100.

(GEE) [11]. Acquisition dates are $t_1 = 10$ Feb, $t_2 = 10$ Apr, $t_3 = 16$ May, $t_4 = 15$ Jul, $t_5 = 1$ Sep, $t_6 = 7$ Oct, and $t_7 = 12$ Nov, all in 2016. Figure 1 shows an RGB representation of the VH data from 10 Feb (red), 15 Jul (green), and 12 Nov (blue), 500 by 800 10 m pixels.

The data acquired in instrument Interferometric Wide Swath (IW) mode, are Sentinel-1 Ground Range Detected (GRD) scenes, processed using the Sentinel-1 Toolbox[3] to

[3]https://sentinel.esa.int/web/sentinel/toolboxes/sentinel-1.

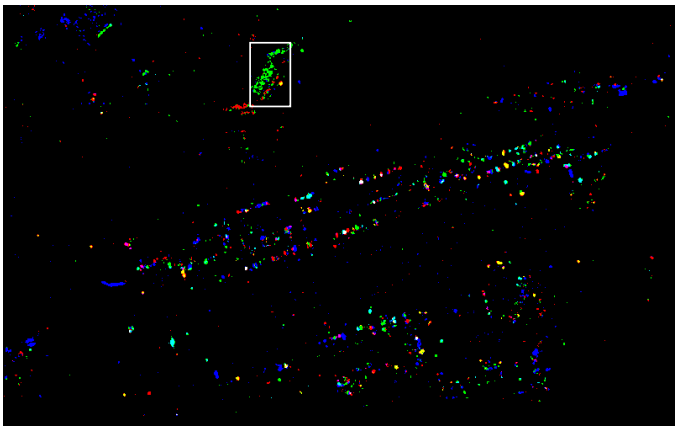

Fig. 3. RGB image of significant change from t_4 to t_5 as red, from t_5 to t_6 as green, and from t_6 to t_7 as blue. Note the green pixels (indicating change in an agricultural field from t_5 to t_6) inside the white rectangle.

generate a calibrated, ortho-corrected product. This processing includes thermal noise removal, radiometric calibration, and terrain correction using Shuttle Radar Topography Mission 30 m (SRTM 30) data. Finally it includes saturating the data (quoting GEE): "Values are then clamped to the 1st and 99th percentile to preserve the dynamic range against anomalous outliers, and quantized to 16 bits." This is to avoid excessive precision loss during conversion from floats to integers for storage. The outliers saturated at the 99th percentile are usually due to strong reflections from sharp angles on antennas and other man-made objects. The spatial resolution is (range by azimuth) 20 m by 22 m and the pixel spacing is 10 m. The IW data are multi-looked, the number of looks is 5 by 1 and the equivalent number of looks is 4.9.

IV. RESULTS

Figure 2 shows the $-2\ln Q$ omnibus change detector for Sentinel-1 C-band VV/VH dual polarization, diagonal only data over the seven time points. No-change regions have low values of $-2\ln Q$, appear dark, and coincide mostly with wooded areas. Change regions have high values of $-2\ln Q$, appear bright, and are primarily due to aircraft coming and going to and from gates and aprons in the airport. Apart from these conspicuous changes, some change is associated with agricultural activities to the north and the north-west of the airport near the town of Kelsterbach.

To give an example on change in the agricultural areas, Figure 3 shows an RGB image of significant change from t_4 to t_5 as red, from t_5 to t_6 as green, and from t_6 to t_7 as blue.

TABLE II. AVERAGE NO-CHANGE PROBABILITIES FOR THE FIELD INSIDE THE WHITE RECTANGLE IN FIGURE 3; THE ONLY CHANGE IS MARKED IN YELLOW.

	$t_1 = \cdots = t_7$	$t_2 = \cdots = t_7$	$t_3 = \cdots = t_7$	$t_4 = \cdots = t_7$	$t_5 = t_6 = t_7$	$t_6 = t_7$
Omnibus	0.0089	0.0161	0.0204	0.1275	0.1534	0.2385
$t_1 = t_2$	0.4946					
$t_2 = t_3$	0.4453	0.5076				
$t_3 = t_4$	0.2455	0.2569	0.2353			
$t_4 = t_5$	0.1991	0.2314	0.2625	0.4761		
$t_5 = t_6$	0.0059	0.0104	0.0176	0.0809	0.1417	
$t_6 = t_7$	0.1186	0.1370	0.1872	0.3908	0.3984	0.2385

Change probability significance level is 0.9999. Specifically, note the green pixels (indicating change from t_5 to t_6) inside the white rectangle. (There is no significant change at this level in these pixels before t_5.) Table II shows the average no-change probabilities for this field (the green pixels inside the white rectangle in Figure 3). This table confirms that change in the field occurred from t_5 to t_6 only: p-values in the $t_1 = \cdots = t_7$ column shows change between t_5 and t_6 only, the p-value is 0.0059 (marked in yellow), and the p-value in the $t_6 = t_7$ column for change between t_6 and t_7 is 0.2385, i.e., no change.

Saturating the extreme pixel values as done presently in GEE is unfortunate in our situation where the dominating changes detected are due precisely to those strongly reflecting man-made objects mentioned in Section III, namely aircraft. Pixels that are saturated at several time points may not be detected as change pixels, which is potentially wrong. The best way to handle this is to store the data as floats but of course this would double the amount of storage required in the GEE data archive.

Further, the Wishart distribution applied is valid in principle only for fully developed speckle which we do not have for aircraft. This led us to perform a small test (not shown here) where we had the same type of Sentinel-1 data as here for three time points over a military aircraft graveyard at the Davis-Monthan Air Force Base in Tuscon, Arizona, USA. As opposed to results from the analysis in this paper, the non-moving aircraft in the three time point case were not detected as change. This gives us confidence in the validity of the results described in this paper.

V. CONCLUSIONS

The omnibus analysis in a satisfactory fashion points to areas of high change in the Sentinel-1 data over the seven time points, namely where aircraft come and go at the airport's gates and aprons. It also shows some change in agricultural areas.

Storing the data in 16 bits with saturation of extreme pixels to avoid loss of dynamics as done presently in Google Earth Engine is unfortunate. This is especially true in this case where the most conspicuous change is associated with high and therefore potentially saturated values.

The Wishart distribution is not ideal for man-made objects such as aircraft. However, based on a small study with stationary aircraft we have confidence in the results obtained.

The ability of the method to detect and isolate regions of intense activity (here the coming and going aircraft), together with the ongoing availability of Sentinel imagery, suggest applications in the area of remote monitoring, for example in the verification of arms control and disarmament agreements, see for instance [12].

Matlab and Python code to perform this kind of analysis is available [10].

REFERENCES

[1] K. Conradsen, A. A. Nielsen, and H. Skriver, "Determining the points of change in time series of polarimetric SAR data," *IEEE Transactions on Geoscience and Remote Sensing*, vol. 54, no. 5, pp. 3007–3024, May 2016, http://www.imm.dtu.dk/pubdb/p.php?6825.

[2] J. J. van Zyl and F. T. Ulaby, "Scattering matrix representation for simple targets," in *Radar Polarimetry for Geoscience Applications*, F. T. Ulaby and C. Elachi, Eds. Artech, Norwood, MA, 1990.

[3] K. Conradsen, A. A. Nielsen, J. Schou, and H. Skriver, "A test statistic in the complex Wishart distribution and its application to change detection in polarimetric SAR data," *IEEE Transactions on Geoscience and Remote Sensing*, vol. 41, no. 1, pp. 4–19, Jan. 2003, http://www.imm.dtu.dk/pubdb/p.php?1219.

[4] M. J. Canty, *Image Analysis, Classification and Change Detection in Remote Sensing. With Algorithms for ENVI/IDL and Python*, Taylor & Francis, CRC Press, third edition, 2014.

[5] V. Akbari, S. N. Anfinsen, A. P. Doulgeris, T. Eltoft, G. Moser, and S. B. Serpico, "Polarimetric SAR change detection with the complex Hotelling-Lawley trace statistic," *IEEE Transactions on Geoscience and Remote Sensing*, vol. 54, no. 7, pp. 3953–3966, Jul. 2016.

[6] A. A. Nielsen, M. J. Canty, H. Skriver, and K. Conradsen, "Change detection in multi-temporal dual polarization Sentinel-1 data," in *International Geoscience and Remote Sensing Symposium (IGARSS)*, Fort Worth, Texas, USA, Jul. 2017, IEEE, Accepted.

[7] J. Schou, H. Skriver, A. A. Nielsen, and K. Conradsen, "CFAR edge detector for polarimetric SAR images," *IEEE Transactions on Geoscience and Remote Sensing*, vol. 41, no. 1, pp. 20–32, Jan. 2003, http://www.imm.dtu.dk/pubdb/p.php?1224.

[8] A. A. Nielsen, K. Conradsen, and H. Skriver, "Change detection in full and dual polarization, single- and multi-frequency SAR data," *IEEE Journal of Selected Topics in Applied Earth Observations and Remote Sensing*, vol. 8, no. 8, pp. 4041–4048, Aug. 2015, http://www.imm.dtu.dk/pubdb/p.php?6827.

[9] T. W. Anderson, *An Introduction to Multivariate Statistical Analysis*, John Wiley, New York, third edition, 2003.

[10] A. A. Nielsen, K. Conradsen, H. Skriver, and M. J. Canty, "Visualization of and software for omnibus test based change detected in a time series of polarimetric SAR data," *Submitted*, 2017, http://www.imm.dtu.dk/pubdb/p.php?6914.

[11] Google Earth Engine Team, "Google Earth Engine: A planetary-scale geo-spatial analysis platform," https://earthengine.google.com, 12 2015.

[12] M. Canty, B. Jasani, I. Lingenfelder, A. A. Nielsen, I. Niemeyer, S. Nussbaum, J. Schlittenhardt, M. Shimoni, and H. Skriver, "Treaty monitoring," in *Remote Sensing from Space – Supporting International Peace and Security*, B. Jasani, M. Pesaresi, S. Schneiderbauer, and G. Zeug, Eds., chapter 12, pp. 167–188. Springer, 2009.